

A Procedure for Correcting the Apparent Optical Depths of Moderately Saturated Interstellar Absorption Lines

Edward B. Jenkins

Princeton University Observatory

Princeton, NJ 08544-1001; ebj@astro.princeton.edu

ABSTRACT

Presently, most observations of absorption lines from interstellar and intergalactic matter have sufficient resolution to show most of the structure at differing radial velocities of the absorber. This added information allows one to go beyond the practice of just obtaining equivalent widths. As with measurements of W_λ , however, it is important to sense and correct for the fact that some parts of a profile may arise from absorption peaks that are strong enough to be saturated. This effect may be unrecognized, or at least underappreciated, in those cases where the narrowest velocity structures are degraded by the convolution of the true spectrum by the instrumental profile.

Using a procedure that is virtually identical to the curve of growth method for equivalent widths, one can compare at any velocity the apparent optical depths τ_a of two lines that have significantly different transition probabilities. If their ratio is smaller than the ratio of the lines' values of $f\lambda$, the actual saturation is more severe than that indicated by the values of τ_a . This paper describes a simple procedure for selectively boosting τ_a of the weaker of the two lines so that unresolved saturated structure is accounted for. This enables one to obtain a very nearly correct answer for the column density per unit velocity. (The lost velocity detail is not restored however.) Two synthetic, test examples of very complex, saturated profiles are analyzed with this method to show how well it works. A demonstration with real observations is also presented. An explicit, easily-computed formula that is a very close approximation to the real correction factors is given, to make data analysis and error estimation more convenient.

Subject headings: ISM: abundances — methods: data analysis — techniques: spectroscopic

1. Introduction

Over recent years, improvements in spectrographs and detectors have brought forth substantial gains in the quality of observations of absorption features arising from either interstellar gases in front of stars in our Galaxy or material in very distant systems in front of quasars. Most modern observations of these features have good signal-to-noise ratios, accurate determinations of the zero intensity level, and sufficient wavelength resolution to break the overall absorption profiles into subcomponents at different Doppler shifts. These advances have allowed us to progress beyond the simple practice of measuring and interpreting just the total equivalent widths of the absorptions. Now, with the ability to discern the added dimension of velocity in the absorption features, an observer is presented with new opportunities for more detailed interpretations. With this expansion, however, come new challenges and responsibilities, ones that extend beyond the framework of analysis techniques that were connected with equivalent widths.

Except for features that we are sure must arise from regions with elevated temperatures, we are rarely confident that all of the substructures within the radial velocity peaks have been completely discerned by the spectrograph. There is evidence that, as a rule, observations taken at successively higher resolutions reveal finer details than those registered before; good examples can be seen in the interstellar Na I absorption features recorded by Wayte, Wynne-Jones & Blades (1978), Blades, Wynne-Jones & Wayte (1980), Welty, Hobbs & Kulkarni (1994) and Barlow, et al. (1995) and some molecular lines observed by Crawford, et al. (1994) and Crane, Lambert & Sheffer (1995). Ultimately, the intrinsic dispersion of Doppler velocities (partly thermal, partly turbulent) may be the only limiting factor in the fineness of the real features. With typical temperatures of cool gas complexes extending below 100K and negligible turbulence, we can expect velocity dispersion parameters b that could be as small as 0.2 km s^{-1} (for atoms with a mass of about 40 amu), a value that is still significantly narrower than most present-day instrumental profiles. Unfortunately, as we shall see in the discussion that follows, the consequences of instrumental smoothing are more serious than just a loss of velocity detail. Observers must often face the challenge of determining how badly saturated the absorptions were before the smoothing took place. This is an important step in deriving trustworthy conclusions about the amount of material that caused the absorption.

An observer's ultimate objective is usually to determine not only the total column density N of an absorber, but also how the atoms, ions or molecules are distributed over different radial velocities. For the original form of the spectrum $I(v)$ that has not been degraded by a convolution with the instrumental profile, the column density as a function of Doppler velocity $v = (\lambda - \lambda_0)/(c\lambda_0)$ is equal to the absorption feature's optical depth

$\tau(v) = \ln[I_0/I(v)]$ multiplied by the constant factor $(m_e c)/(\pi e^2 f \lambda)$ (I_0 is the intensity of the unabsorbed continuum). What one observes in actual practice, however, is an apparent intensity $I_a(v)$ that is a smoothed form of the real intensity profile $I(v)$. Even so, as long as the smoothing is not too severe, one can derive an approximate representation that is called the *apparent* optical depth $\tau_a(\lambda) = \ln[I_0/I_a(v)]$, an interpretative concept first used for high resolution recordings of lines in the visible part of the spectrum by Hobbs (1971, 1972, 1973, 1974a, b) and later invoked for UV lines by Savage, et al. (1989), Jenkins, et al. (1989), Savage, Massa & Sembach (1990), Joseph & Jenkins (1991), Sembach, Savage & Massa (1991) and Tripp, Sembach & Savage (1993) in their analysis of some IUE and IMAPS data. More recently, spectra of exceptionally good quality and resolution have been produced by the GHRS echelle spectrograph on the Hubble Space Telescope, and representations of τ_a have been important tools for understanding these data (Cardelli et al. 1991; Savage et al. 1991; Savage, Cardelli, & Sofia 1992; Sofia, Savage, & Cardelli 1993; Savage, Sembach, & Cardelli 1994; Cardelli & Savage 1995). Important properties of τ_a have been explained in detail by Savage & Sembach (1991).

The papers cited above have made it clear that apparent optical depths are useful functions for deriving column densities and extracting linear representations for all of the kinematical information that is available. The information conveyed by the τ_a functions represents a significant improvement over the single numbers that signify the equivalent widths of entire profiles or resolved pieces of profiles. Nevertheless, we must be aware of some limitations that arise in certain circumstances (Jenkins et al. 1989; Joseph & Jenkins 1991). The real physical processes that created the recorded intensities consisted of an exponential attenuation of the light, followed by an instrumental smearing of the spectrum. The derivation of τ_a is an attempt to reconstruct a linear representation for the amount of absorbing material by unraveling the exponential absorption law, but it disregards the convolution by the instrumental profile that followed. Normally, we are accustomed to interpreting functions where there is simply a loss of detail caused by smoothing. But unfortunately τ_a does *not* represent just a smoothed version of the real τ . Instead, we find that the smoothing has deaccentuated the extremes in τ , and the nonlinear operation used to construct τ_a creates a representation of τ that is both smoothed *and distorted*. There are only two circumstances where τ_a represents an unbiased reflection of the sought-after distribution: (1) All of the velocity details of the profile were fully resolved so that τ_a is identical to τ , or (2) $\tau \ll 1$ everywhere, so that the $\ln[I_0/I(\lambda)]$ is essentially equivalent to the linear representation $[I_0 - I(\lambda)]/I_0$ whose integral over any λ interval is not changed by the convolution operation. In the first case, all of the information is recovered, while in the second, the only repercussion is a loss of velocity detail.

In short, in the course of interpreting $\tau_a(v)$ an observer must be vigilant about the pos-

sible loss of evidence that narrow peaks in absorption are badly saturated. There is a danger that instrumental smearing has created a picture where the reduction of intensity *appears* to be weak and thus far from saturation. The same argument holds for stronger features. Even if one can sense that some saturation must be evident because the intensity is significantly below the continuum level, smoothing of the bumps could cause one to underestimate its severity and then misjudge the actual amount of material in the line of sight.

A straightforward way to sense and measure the amount of hidden saturation is to observe two or more lines with differing transition probabilities from the same species. If, at any velocity v , the apparent optical depths in the smoothed spectra exhibit a scaling that is weaker than the progression of the respective lines' $f\lambda$ values, then there is good reason to believe that in some places the unresolved saturated structures are stronger than a general level suggested by the apparent (smoothed) intensity values. The object of this paper is to demonstrate how one can correct for this effect and derive reasonably accurate representations of column density as a function of velocity. The method to be outlined has a relationship with the conventional curve of growth analysis for equivalent widths that is stronger than just a simple analogy. As the arguments in §2 will show, the two methods have nearly identical mathematical foundations. The principal advantage of correcting τ_a rather than W_λ is that we do not sacrifice the information contained in velocity peaks that can be resolved. Hence one can explore, for instance, how the abundances of different species change with velocity, rather than just determining the overall abundance ratios at all velocities within some large complex of components.

In their instructive overview on how to derive, interpret and exploit the apparent optical depths of interstellar features, Savage & Sembach (1991) likewise addressed the problem of how to cope with the misrepresentations of the real optical depth levels caused by instrumental smearing. They proposed that one should measure the disparity in inferred column densities *integrated over velocity* for two lines and then apply, according to a specific prescription, a global, multiplicative (upward) correction to the entire profile of the weaker line.¹ The method advocated here uses a different approach that is an improvement over the one described by Sembach & Savage. Corrections are applied on the spot at individual velocities, without regard to what is happening elsewhere. The two methods will be compared in §4.

A very different tactic for analyzing saturated, blended features is to build a model of the real absorption complex by defining such parameters as the strengths, widths and velocity centroids of individual components (Vidal-Madjar et al. 1977; Ferlet et al. 1980;

¹This correction procedure may be applied to any two lines of arbitrarily different strengths (within reason), but Savage & Sembach supplied correction factors only for lines that had a 2:1 ratio for $f\lambda$.

Welsh, Vedder, & Vallerga 1990; Hobbs & Welty 1991; Welsh et al. 1991; Welty, Hobbs, & York 1991; Spitzer & Fitzpatrick 1993, 1995; Vallerga et al. 1993; Fitzpatrick & Spitzer 1994; Welty, Hobbs, & Kulkarni 1994; Crane, Lambert, & Sheffer 1995). One then solves (or searches) for a minimum in the χ^2 values as parameters for the theoretical representation of the instrumentally blended complex are compared with the observations. In cases where independent information can help to constrain the choice of free parameters (such as much higher resolution observations of other species), this method can be successful. While such model building has the potential of helping us to understand some details that may not be evident in a display of smoothed optical depths, it has the disadvantage of usually relying on human judgement to define the constraints on the parameters and the method of converging to a minimum χ^2 . Also, the models contain specific assumptions about the functional forms of the components, with the usual choice being a Gaussian (or Voigt) profile. By contrast, the derivation of τ_a is a simple, mechanical process that places no such requirements on the investigator and does not rely on any specific models, even when the corrections discussed later in this paper are implemented.

2. Basic Concepts

For the purposes of discussion, we shall address the problem of working with the optical depths of two lines that have values of $f\lambda$ that differ by a factor of 2. This situation is frequently encountered in astronomical spectroscopy, such as when the strong $^2\text{S} - ^2\text{P}^0$ resonance doublets of lithium-like atoms and ions are observed. The arguments apply equally well to other line strength ratios, within reasonable limits that are set by errors that arise either from noise or systematic measurement problems.

In §2.1 below, we start with a trivial example of how to analyze a single Gaussian profile. In sections that follow, we make use of some simple theorems to address progressively more complex situations, ending up with arbitrarily strong profiles with very complicated shapes.

2.1. A Single, Saturated Gaussian Profile

Before approaching the problem of correcting optical depths, we should first review the basic principles of the doublet ratio method (Unsöld, Struve, & Elvey 1930; Beals 1936; Wilson & Merrill 1937; Strömngren 1948), a classical analysis that is applied to the equivalent widths of the two members of a doublet. Strictly speaking, the analysis is correct only for a Voigt intensity profile created by a Gaussian 1-dimensional velocity distribution (or two or

more such profiles caused by *identical*, well separated Gaussian components). In practical situations where there is no better choice, it is customary for investigators to make the implicit assumption that the velocity structure of the absorbing material is very similar to that of a single Gaussian. When a line is optically thin everywhere

$$\frac{W_\lambda}{\lambda} = \frac{\pi e^2 f \lambda N}{m_e c^2}. \quad (1)$$

However when there is enough material and a low enough velocity dispersion b to make the lines saturated, any line with a central optical depth

$$\tau_0 = \frac{\pi^{1/2} e^2 f \lambda}{m_e c} \left(\frac{N}{b} \right) \quad (2)$$

should have an equivalent width given by

$$\frac{W_\lambda}{\lambda} = \frac{2bF(\tau_0)}{c} \quad (3)$$

where

$$\begin{aligned} F(\tau_0) &= \int_0^\infty [1 - \exp(-\tau_0 e^{-x^2})] dx \\ &= \frac{\pi^{1/2}}{2} \sum_{n=1}^\infty \frac{(-1)^{n-1} \tau_0^n}{n! n^{1/2}}. \end{aligned} \quad (4)$$

From the ratio

$$R = F(2\tau_0)/F(\tau_0) \quad (5)$$

of the doublet's two equivalent widths, one can calculate a correction factor

$$C_R = \frac{\pi^{1/2} \tau_0}{2F(\tau_0)} \quad (6)$$

that would be needed to enhance the weaker line's W_λ so that Eq. 1 for low optical depths would apply. (In this case, τ_0 is the central optical depth of the weak line and the factor 2 in Eq. 5 reflects the ratio of the two lines' $f\lambda$ values.)

Now that the concept of doublet ratio corrections has been introduced, we move on to address how we would operate with the two $\tau_a(v)$ functions instead of just a pair of numbers representing the absorption over all velocity, i.e., the two W_λ 's. Again, we consider an observation of moderately saturated lines in a (2:1) doublet, where the column density of the absorber has a velocity distribution that is a single Gaussian and the feature has a central optical depth τ_0 for the weaker line.

In the limit where the instrumental profile is very much broader than the widths of the lines, the two smoothed absorption functions $[I_0 - I_a(v)]/I_0$ have several important properties. First, they have shapes that are virtually identical to the instrumental smearing function and areas equal to the lines' equivalent widths. Second, by virtue of the fact that the extreme smearing has degraded the amplitudes of these functions so that their peak values are very much less than one, they are close approximations to the $\tau_a(v)$ functions. It then follows that at every v the ratios of the two lines' $\tau_a(v)$'s are identical to the ratio of the equivalent widths. If we now take this ratio R and solve Eqs. 4 and 5 to find τ_0 , we may derive the correction factor from Eq. 6 and evaluate N according to

$$N = \frac{m_e c}{\pi e^2 f \lambda} \int C_R \tau_a(v) dv, \quad (7)$$

where here $C_R \tau_a(v)$ replaces $\tau(v)$ in the usual equation for deriving N from the integral of a true optical depth over all velocity. While this cumbersome procedure for obtaining N is mathematically equivalent to invoking the doublet ratio method on equivalent widths, it serves as a trivial but good introductory illustration of the principle of correcting $\tau_a(v)$.

If we move to the opposite extreme of having a smearing function that is much narrower than the velocity spread of $\tau(v)$, we find that $\tau_a(v)$ of the strong line is always twice the value of $\tau_a(v)$ of the weak line because $\tau_a(v)$ is practically identical to the true $\tau(v)$. Here, one would obtain N by evaluating Eq. 7 with $C_R = 1$.

In the two preceding extreme cases of very poor and very good resolution, C_R does not change with v . In the intermediate case where the line is only partly degraded by instrumental smearing, both R and C_R vary. (Henceforth, we will work with a modified notation $R(v)$ and $C_R(v)$ as a reminder that these quantities change with velocity). Also, it is no longer possible to show by elementary arguments that a point-by-point correction will indeed make Eq. 7 work. In fact, numerical simulations indicate that for a single Gaussian with $\tau_0 = 3.4$ for the weak line, Eq. 7 overestimates N by 4% in the worst possible case of intermediate resolution.²

2.2. A Cluster of Nonoverlapping Gaussians

We now consider the problem of analyzing several Gaussian profiles that are blended together by the instrument, but that are actually well separated from each other in the absence of such blending. The key to solving this problem relies on an interesting property

²This occurs when the FWHM of a Gaussian instrumental profile is equal to $1.5b$.

of the combined strengths of saturated lines noted by Jenkins (1986). He demonstrated that the application of a curve of growth (or doublet ratio) analysis to a sum of the equivalent widths of an ensemble of Gaussian profiles, while technically an incorrect procedure, still gives an answer for the sum of N over all of the contributions that is usually only slightly below the correct value. The method works satisfactorily even when there is a significant dispersion in the τ_0 and b values for the separate components. For example, when the doublet ratio analysis is tried on the two sums of equivalent widths of population of lines that have an average central optical depth for the weak line $\langle\tau_0\rangle = 4$ but with an rms dispersion of 40% for the individual τ_0 's and b 's, the standard calculation for the total value of N should, on average, be equal to 94% of the true value. Lower values for either $\langle\tau_0\rangle$ or the dispersion of τ_0 give results that are closer to the true one. The only condition where the analysis breaks down seriously is when the distribution of τ_0 or b is markedly bimodal (or when there are so few components that small-number statistical fluctuations may be important).

From the findings presented in the above paragraph and reasoning given in §2.1, we can see that a severely underresolved recording of a sparse cluster of saturated Gaussian profiles can be treated in the same manner as a single Gaussian. Once again, we evaluate the correction factor $C_R(v)$ everywhere, and, through the use of Eq. 7, obtain the column density for the entire group. This argument applies even if the cluster of features spans a velocity interval that is much larger than the instrumental profile. In this case, the value of $\tau_a(v)$ at any point represents simply a weighted sum of the equivalent widths of a bunch of lines on either side of v . The derived differential value of N at this velocity will reflect, with reasonable accuracy, the amount of material present in these components, after their contributions have been multiplied by the same weight factors.

As with the single Gaussian, an observation that fully resolves the individual components will yield $C_R(v) = 1$ everywhere, with the outcome that $\tau_a(v)$ needs no upward correction because it is virtually the same as $\tau(v)$. Only in the case where the resolving power is roughly comparable to the line widths do we face the prospect of having a mild inaccuracy in the answer.

2.3. A Dense Cluster of Overlapping Gaussian Profiles

Suppose that we now enhance the absorption of the sparse complex of lines by adding many new components, all of which have the same population characteristics as before. If the complex's velocity span remains constant, we could reach a point where the lines start to overlap each other. Going still further, new components could be added to the point that they pile on top of each other many times over. We are now presented with an overall

absorption profile that is very complex and, on average, with a depth $I_0 - I_a(v)$ that could now be a very significant fraction of the continuum level I_0 .

In real life, if there are no coherent physical processes that can have a dynamical influence on the radial velocities of the components, one can expect the small-scale placement of the components' velocity centroids to be random. When this is the case, the average optical depth will grow in direct proportion to the density of components per unit velocity. In essence, Beer's law is operating on the average amount of flux that is permitted to penetrate a random superposition of absorbers.³ This behavior insures that $\tau_a(v)$ will continue to represent, within the instrument's passband centered on v , a (weighted) sum of equivalent widths of the components, i.e., the W_λ 's that would have been accumulated in the absence of any mutual obstruction of the lines. The situation here is therefore no different than that presented in §2.2, except that the $\tau_a(v)$'s are no longer much less than 1. It follows from the proportionality of line density to average optical depth that the evolution of a given population of components from a sparse to a dense cluster has no effect on either $R(v)$ or the factor $C_R(v)$ that is needed to boost the equivalent widths (and hence $\tau_a(v)$) to a value that approximately represents the smoothed $\tau(v)$.

3. A Demonstration

Now that the basic principles of correcting $\tau_a(v)$ have been presented, it is appropriate to create some test cases that demonstrate how the method works. Two examples will be offered. The first will consist of a 60 km s⁻¹ wide complex of mostly saturated Gaussian lines, all different from each other, whose narrowest members are distributed sparsely enough to create only occasional overlaps. The second example will contain a much denser collection with many more such lines. The second example will have a density of components per unit velocity that is large enough to cause a substantial compounding of absorptions at most velocities. These two examples are tailored to illustrate the principles discussed in § 2.2 and § 2.3, respectively.

Certain properties of the line complexes were contrived to serve a useful pedagogical purpose, but at some expense in realism. For instance, Fig. 1 shows the values of central

³By analogy, one can picture the attenuation of light passing through a forest. Averaged over some solid angle of reasonable size, we expect an exponential attenuation law to apply, even when there is a mix of large and small trees and, moreover, some of the trees are opaque while others are translucent. (However, in contrast to a natural forest, a commercial tree farm does not obey this principle because there is some regularity in the locations of the trees.)

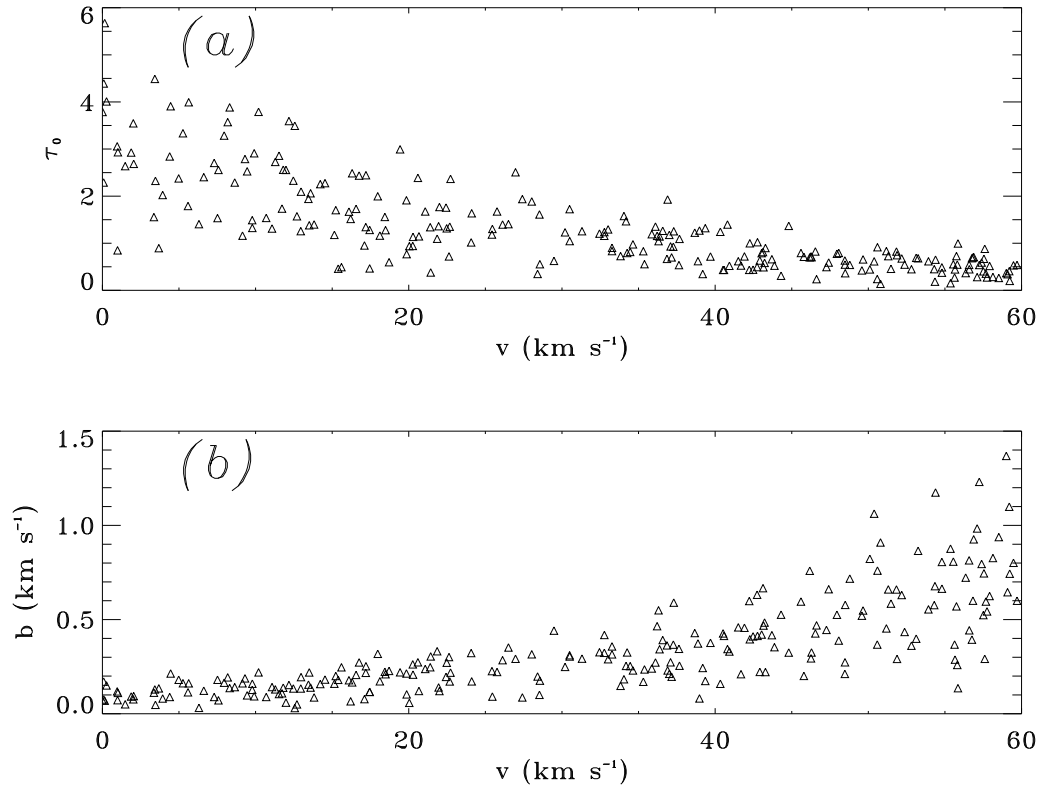


Fig. 1.— Central optical depths τ_0 (panel *a*) and velocity dispersions b (panel *b*) of contributions that made up the dense line complex demonstration example, as a function of the locations of the lines' central velocities.

optical depths and velocity dispersions of components as a function of their location (velocity) within the dense absorption complex. (The sparse complex is just a small subset from the same general population.) In both cases, the complexes were constructed such that the average central optical depths $\langle\tau_0\rangle$ decreased from left to right, while at the same time the average velocity widths $\langle b\rangle$ increased to make the product $\langle\tau_0\rangle\langle b\rangle$ constant over the entire velocity span. One could imagine this absorption complex arising from some fictitious case where a heterogeneous collection of interstellar clouds had a steady increase in kinetic temperature as the radial velocities progressed from 0 to 60 km s⁻¹. Within any small velocity interval, the dispersions of τ_0 and b were constructed to be equal to 40% of their mean values (but with a cutoff at -2σ to prevent negative or inordinately low values). The top two panels (*a* and *b*) in Fig. 2 show the original, fully resolved intensities of the weak transition for the sparse and dense ensembles, before they were smoothed by an instrumental profile that consists of a Gaussian with a FWHM = 2 km s⁻¹. Immediately below these panels are the smoothed forms for both the strong and weak lines. The intensities are converted to apparent optical depths and shown in the next row of panels. In both cases, the last pair of panels show that the ratios $R(v)$ of the two optical depths progress in a somewhat irregular fashion from about 1.2 on the left hand side to about 1.9 on the right. The fluctuations on top of the general trend are caused by random changes in the relative mix of lines with different degrees of saturation.

At each velocity v , we measure $R(v)$, the ratio of the strong line’s $\tau_a(v)$ to that of the weak one, and derive $C_R(v)$ by solving Eqs. 5 and 6 (a streamlined way of directly computing $C_R(v)$ will be presented in § 6). The results are shown in Fig. 3. On the left hand side where the individual components are narrow and saturated, $\tau_a(v)$ (shown by the dotted line) is significantly below a smoothed version of the true optical depth $\tau(v)$ (solid line). Toward the right, the individual components become less saturated but broader, and this reduces the disparity. Note, however, that apart from small-scale random fluctuations, a running average of the true optical depths (and hence column density) does not systematically change from left to right.

After multiplying $\tau_a(v)$ by $C_R(v)$, we obtain a corrected optical depth (dashed line in Fig. 3) that is a good approximation to the smoothed $\tau(v)$ (solid line – the function that we are attempting to reconstruct so that we can derive the column density per unit velocity). The difference between the two is shown by the filled-in curve associated with a baseline that is displaced vertically to a plot y value of -1.5 . In the sparse line case, this error is always less than 0.1 dex, as indicated by the thickness of the black filling. For the dense line example, this error occasionally becomes of order 0.1 dex. These errors are significantly less than the gross underestimates for the smoothed $\tau(v)$ that arise from the raw values of $\tau_a(v)$, as shown by the filled-in curve above the baseline situated at -2.3 in the two panels of the figure. It is

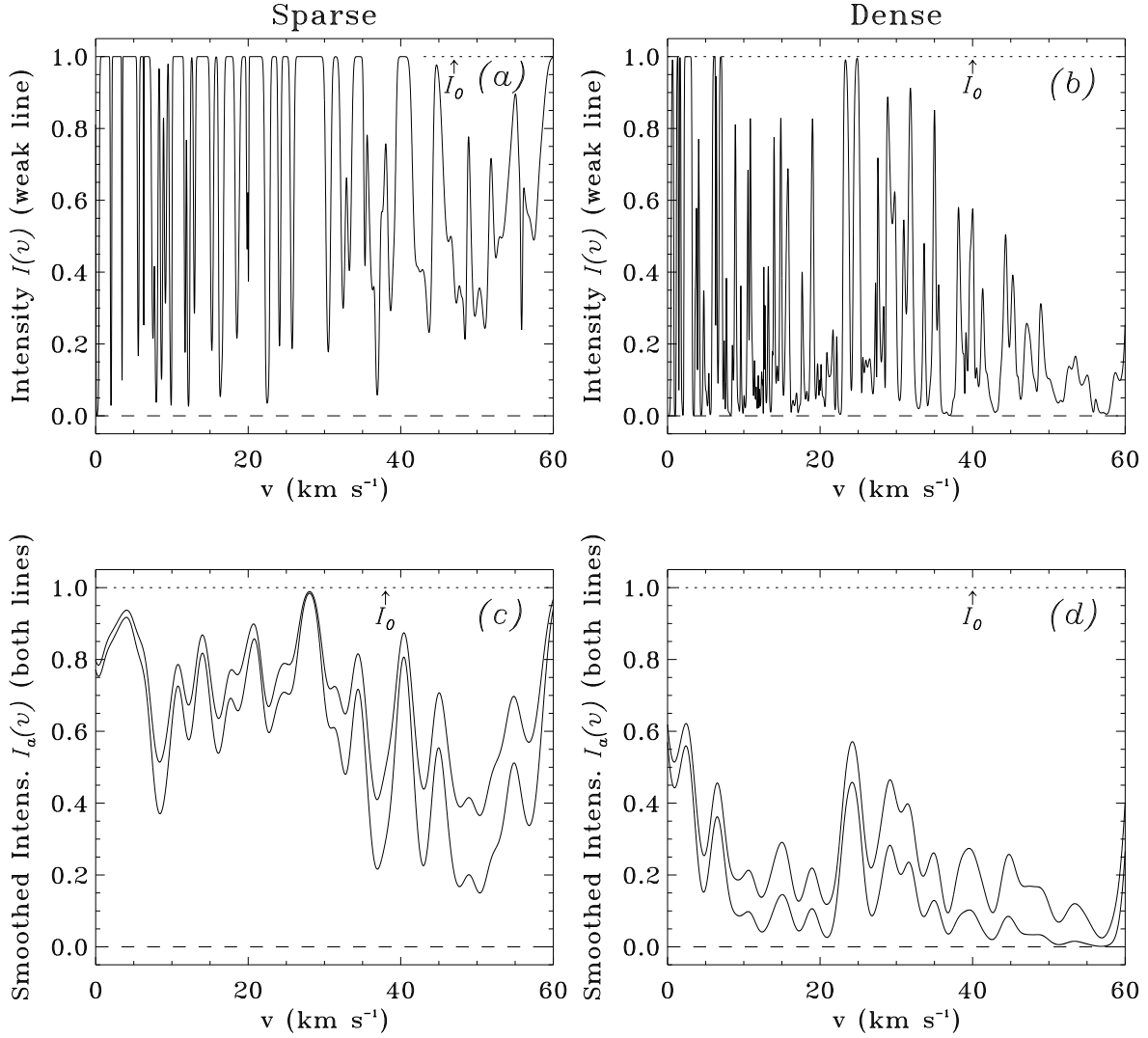


Fig. 2.— Various forms of the two spectral complexes chosen for the demonstration of corrections of $\tau_a(v)$, plotted against radial velocity v . The left-hand panels (*a*, *c*, *e* and *g*) apply to the sparse layout of spectral components, while the right-hand ones (*b*, *d*, *f* and *h*) depict the dense complex. From top to bottom are displayed, (*a* and *b*) the intensities of the weak line before instrumental smoothing, (*c* and *d*) the intensities of both lines after they have been smoothed by the instrument (upper curve: weak line, lower curve: strong line), (*e* and *f*) the derived values of $\tau_a(v)$ (lower curve: weak line, upper curve: strong line), and (*g* and *h*) the ratios of the two $\tau_a(v)$'s. The low values of $R(v)$ on the left-hand side, relative to those on the right, indicate the need for a stronger correction $C_R(v)$ for the ensembles of individual components that are deeper and narrower.

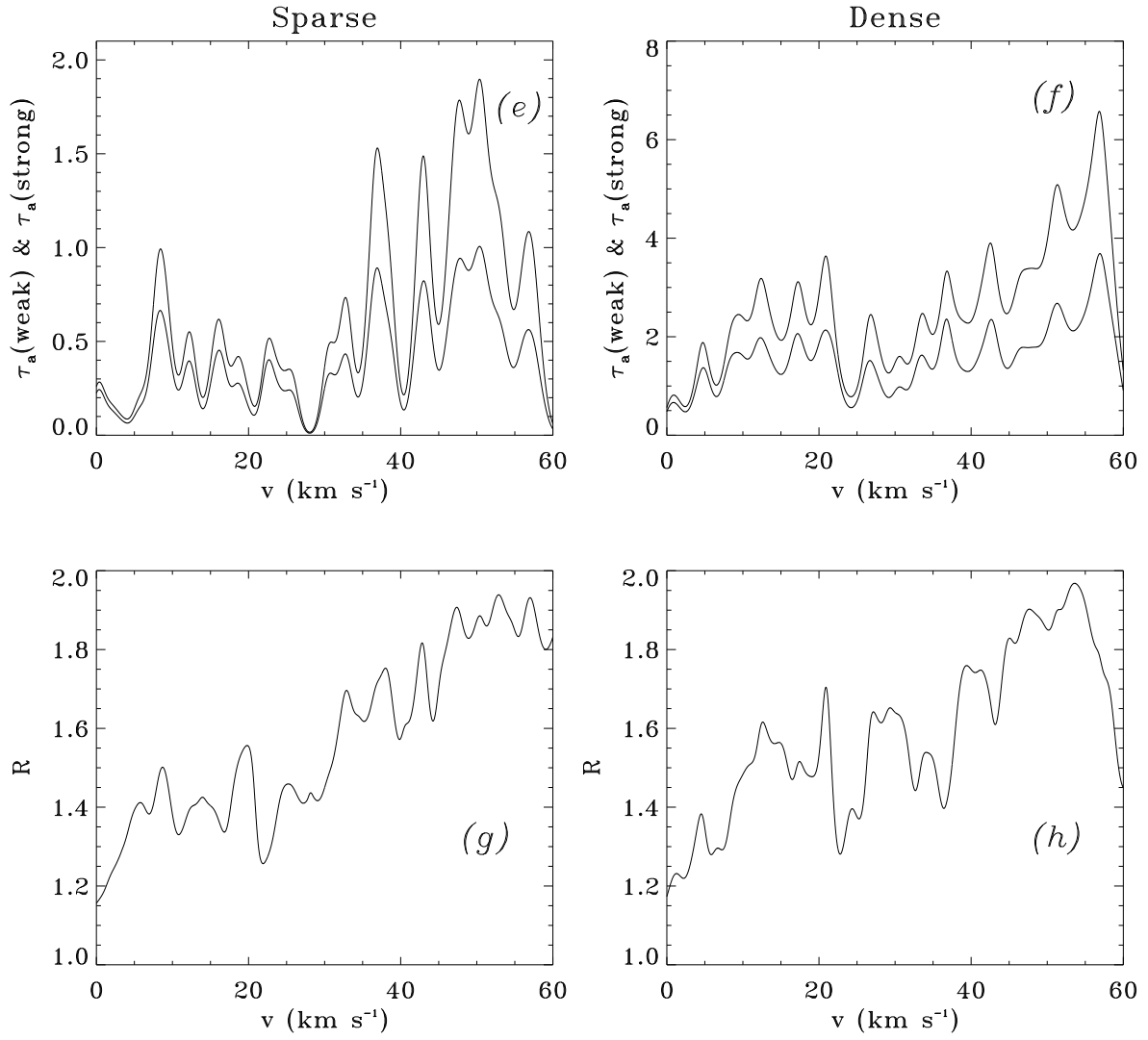


Fig. 2.— continued.

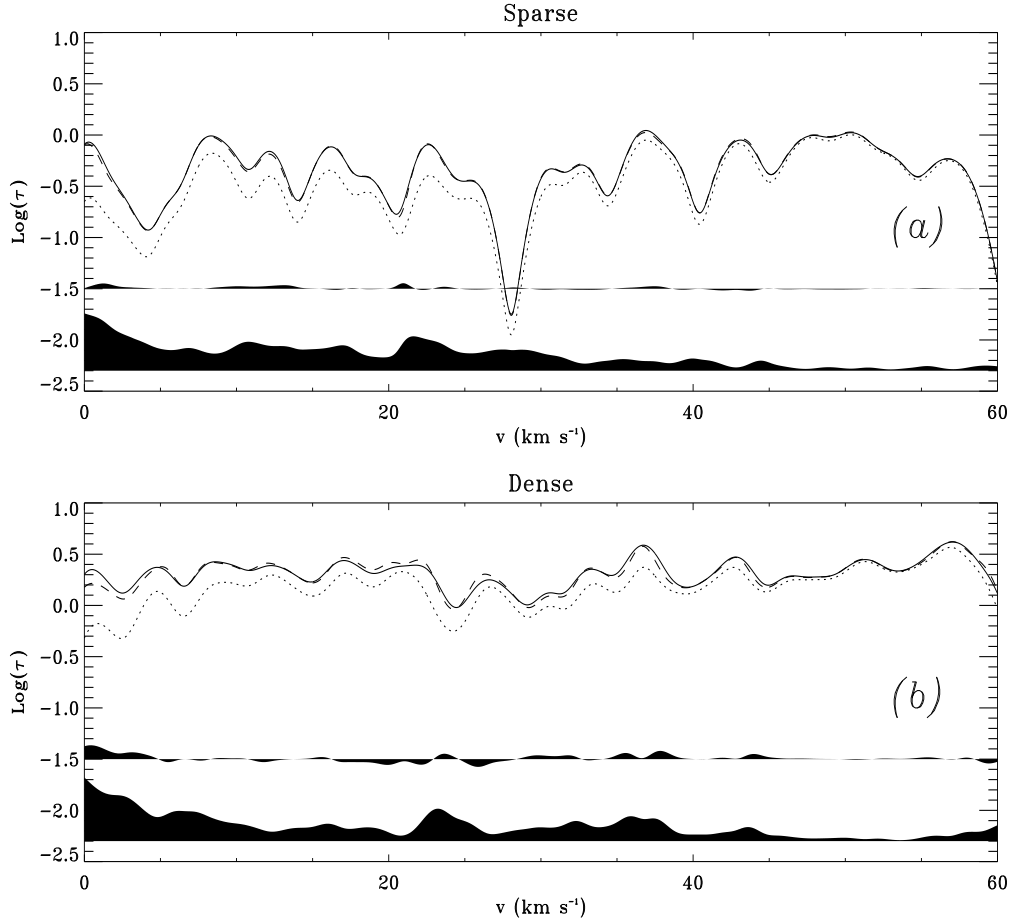


Fig. 3.— Outcomes from the analyses of the sparsely (*a*) and densely populated (*b*) demonstration examples. Logarithmic representations of various forms of the the weak line’s τ ’s are shown as a function of radial velocity v . In each panel of the figure, the solid line shows a smoothed version of the real $\tau(v)$ (not known to an observer). The dotted line is the raw, uncorrected $\tau_a(v)$. The dashed line, often so close to the solid line that it can not be seen, represents the corrected apparent optical depth, $C_R(v)\tau_a(v)$. The curve that encloses the solid shading above the horizontal line at an ordinate of -2.3 illustrates the magnitude of the error in the uncorrected $\tau_a(v)$, i.e., the function shown is $\tau(v)_{\text{smoothed}} - \tau_a(v) - 2.3$. Just above this curve is shown the much smaller error that arises after the $\tau_a(v)$ has been corrected, i.e., here the plot shows $\tau(v)_{\text{smoothed}} - C_R(v)\tau_a(v) - 1.5$.

important to realize, however, that these tests are being performed under conditions where there is absolutely no noise or systematic errors in defining either a continuum level or zero intensity baseline. Under the circumstances of real observing, one would need to assess the impact of these errors on the reliability of the results.

4. A Comparison with the Method of Savage & Sembach

In the preceding section we have examined the performance of the optical depth correction technique on a broad expanse of many randomly situated Gaussian profiles. It is also useful to test the method on a small clump of a few such profiles. Some test examples constructed by Savage & Sembach (1991) are suitable for this purpose. Their six cases range in complexity from a single Gaussian (their Case 1) to a group of 6 components (their Case 6) that overlap and have values of τ_0 and b that differ by factors of 5 (see their Table 2 for details).

We also wish to examine how well total column densities derived from the on-the-spot corrections discussed here compare with the simple global correction scheme discussed by Savage & Sembach. Basically, they proposed that the total column density (in contrast to the column density per unit velocity) be compensated according to the disparities of apparent column densities from the two lines. It is clear that their technique would be inappropriate for certain configurations, such as the two highly contrived cases presented in §3 or certain real observations [e.g., such as the Fe II absorption lines in the spectrum of π Sco shown by Joseph & Jenkins (1991)]. For the demonstration examples in §3, a correction for the left hand side would not work for the right hand side where practically no correction is needed. However, in some more realistic situations where just a few saturated and unsaturated components are mixed together, the story might be different.

In the limit that the resolving power is extremely poor, the two methods should give identical results (and, conversely, at very high resolution no correction is needed). Differences should be apparent only at intermediate resolutions. Table 1 shows the percentage errors, $100 \times [N_{\text{true}} - N_{\text{computed}}]/N_{\text{true}}$, for both methods, applied to the 6 cases of Savage & Sembach with various scaling factors for the optical depths proportional to 2^n . At a resolution of 10 km s^{-1} the two methods perform about equally, i.e., in 14 of the 24 examples the on-the-spot corrections have a smaller error than global correction method of Savage & Sembach, and for the remaining 10 the converse is true. At 20 km s^{-1} the on-the-spot technique does about twice as well (15 wins vs. 7 losses, with 2 draws), and at 40 km s^{-1} the on-the-spot technique is superior in 21 cases and not so in 3.

Table 1. Percentage Errors^a

n ^b	Case ^c	Weak Line	Smoothing Profile FWHM (km s ⁻¹)		
		Max. τ	10	20	40
2	1	0.4	0.0, -0.3	0.3, -0.3	0.4, -0.2
	2	0.5	0.1, 0.0	0.4, 0.1	0.6, 0.3
	3	0.8	-0.1, -0.7	0.4, -0.8	0.8, -0.5
	4	0.9	0.3, -0.2	1.1, 0.4	2.0, 1.0
	5	0.8	0.3, -0.2	1.2, 0.1	1.7, 0.7
	6	0.4	0.0, 0.9	0.1, -0.1	0.4, -0.2
3	1	0.8	0.0, -0.9	0.4, -0.8	1.0, -0.5
	2	0.9	0.5, -0.1	1.5, 0.4	2.1, 1.0
	3	1.6	-0.5, -2.2	0.1, -1.8	0.5, -1.1
	4	1.8	1.4, -0.1	4.1, 2.4	6.2, 4.6
	5	1.7	1.3, -0.5	4.1, 1.2	5.6, 3.1
	6	0.8	0.1, -0.2	0.3, -0.4	0.8, -0.4
4	1	1.7	-0.7, -2.4	-0.1, -1.7	0.4, -0.9
	2	1.8	2.4, 0.1	5.0, 2.0	6.3, 3.8
	3	3.1	-1.6, -3.3	-2.2, -1.3	-3.6, -0.7
	4	3.5	6.6, 3.1	13.9, 11.2	18.0, 16.2
	5	3.4	6.4, 1.1	12.6, 11.2	15.3, 10.5
	6	1.5	0.7, -0.4	0.8, -0.9	2.3, 0.4
5	1	3.4	-1.0, -2.1	-2.3, 0.0	-4.5, 0.3
	2	3.6	8.7, 3.2	13.6, 8.1	15.0, 10.7
	3	6.3	2.5, 4.0	0.2, 7.0	-3.8, 4.6
	4	7.1	20.9, 16.1	31.4, 28.9	36.2, 34.8
	5	6.7	18.8, 9.8	26.9, 17.9	29.1, 22.7
	6	3.0	2.7, 0.1	3.7, 1.0	9.7, 8.1

^aDouble entries separated by a comma show the error using the method of Savage & Sembach (1991) (first number) and the on-the-spot corrections discussed here (second number). Percentages represent $100 \times [N_{\text{true}} - N_{\text{computed}}]/N_{\text{true}}$, where N is the integrated column density for the entire group of components in each case.

^bExponent of 2 in a multiplicative scale factor for all of the components. See Eq. 12 of Savage & Sembach.

^cIdentification of the particular component group. See Table 2 of Savage & Sembach.

One may notice that the column density correction factors listed by Savage & Sembach (in their Table 4) for adjusting an isolated Gaussian component differ slightly from the C_R that comes from solving Eqs. 5 and 6. For $\log(R/2)$ [$\equiv \log N_a^{n-1} - \log N_a^n$ in the notation of Savage & Sembach] < 0.18 , the two are very close to each other. However if $\log(R/2) = 0.22$, the logarithm of the correction factor for equivalent widths is 0.418, while the corresponding value listed by Savage & Sembach is 0.453. It is possible that the difference is explained by the fact that their correction factors are adjusted slightly to give better performance at intermediate resolving powers. This conclusion seems to be supported by the results shown in Table 1. The method of Savage & Sembach works very well for the pure Gaussian profile (Case 1) and an assemblage of profiles that look very similar to a single Gaussian (Case 3).

5. An Example using Real Observations

As a final demonstration, we explore how well the corrected apparent optical depths reproduce the results of a component model derived from real observations. Spitzer & Fitzpatrick (1993) identified 9 velocity components of S II toward HD 93521 using the absorption profiles from the transitions at 1251\AA ($\log f\lambda = 0.837$) and 1254\AA ($\log f\lambda = 1.136$), along with some supporting information from the absorption features of other species. One can see from their Fig. 2a that these profiles are moderately saturated. However, at the resolution of the GHRS echelle spectrograph, it appears that the lines are fully resolved because $\tau_a(v)$ of the weaker line is, to within observational errors, always equal to half that of the stronger line at all velocities. Thus, no correction is needed, and raw $\tau_a(v)$ values from either line are appropriate for deriving the column density per unit velocity.⁴

To make the demonstration nontrivial and create a disparity in the results for the two transitions, we can smooth the profiles so that they are significantly under-resolved. This smoothing reconstructs how the absorption features would appear if they were observed with a low-resolution spectrograph. The two thin curves in Fig. 4 show the $\tau_a(v)$ relationships for these two S II transitions whose $f\lambda$'s differ by a factor of 2. The $\tau_a(v)$ for the stronger transition was divided by 2 before it was plotted, in order to show how much its implied column density per unit velocity differs from that of the weaker transition.

The heavy line in Fig. 4 shows the corrected $\tau_a(v)$ for the weaker line, i.e., the appearance

⁴This good resolution of the velocity structure by the GHRS echelle spectrograph is not generally achieved when the spectra of stars behind cold clouds are recorded. The line of sight to the high latitude star HD 93521 seems to penetrate only warm material that has components with b values that are generally about equal to or greater than the width of the instrumental profile.

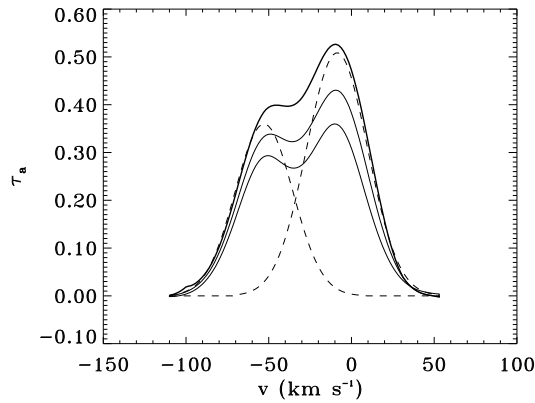


Fig. 4.— Plots of the apparent optical depths of the S II absorption lines in the spectrum of HD 93521, evaluated from the data of Spitzer & Fitzpatrick (1993) after being convolved with a Gaussian profile with a FWHM = 36.7 km s⁻¹ (i.e., $\sigma = 10$ data points) to simulate the effects of smoothing by a low resolution spectrograph. The upper thin curve represents $\tau_a(v)$ for the weak transition at 1251Å, while the lower thin curve is $\tau_a(v)/2$ for the strong one at 1254Å. The thick curve represents $C_R(v)\tau_a(v)$ for the weak line, which can be approximately broken down as a sum of two Gaussian components (dashed curves).

of the line after it has been multiplied by $C_R(v)$. $C_R(v)$ varies from 1.0 to about 1.25 over most of the relevant velocity range of the profiles. An application of Eq. 7 yields $N = 2.14 \times 10^{15} \text{cm}^{-2}$. By comparison, the detailed model for the S II components given by Spitzer & Fitzpatrick gives a total column density of $2.10 \times 10^{15} \text{cm}^{-2}$. If we decompose our corrected $\tau_a(v)$ into two Gaussian components (dashed lines in Fig. 4), we obtain $N = 8.61 \times 10^{14} \text{cm}^{-2}$ for the left-hand one and $N = 1.29 \times 10^{15} \text{cm}^{-2}$ for the one on the right. These values are close to the sums of column densities in two distinct bunches of components in the data of Spitzer & Fitzpatrick. Their components 1–4 had $8.83 \times 10^{14} \text{cm}^{-2}$, and 5–9 had $1.22 \times 10^{15} \text{cm}^{-2}$). Evidently, within the limitations of what can be seen at the low resolution, the profile representing $C_R(v)\tau_a(v)$ is consistent with detailed component fits performed by Spitzer & Fitzpatrick on their high-resolution spectrum.

6. Analytical Approximations for C_R

The solutions to Eqs. 5 and 6 are somewhat awkward to compute in a data reduction program. Thus, as a convenience for observers who wish to undertake an analysis that invokes the corrections for $\tau_a(v)$, some simple analytical approximations for C_R will be presented.

Since these formulae can be differentiated, they are also useful for evaluating how both random and systematic errors respond to the transformations.

It turns out that the relationship between a variable

$$y = \ln(1 + \log C_R) \tag{8}$$

and

$$x = \ln \left[\frac{(f\lambda)_{\text{strong}}}{(f\lambda)_{\text{weak}}} - 1 \right] - \ln(R - 1) \tag{9}$$

is remarkably close to linear. The small departures from linearity can be appropriately handled by a low order polynomial whose coefficients may be evaluated by a least squares fit to the exact calculations. In the practice of reducing real data, we are now free to disregard Eqs. 5 and 6 and, instead, use the much simpler explicit equation

$$\log C_R = \exp(a_0 + a_1x + a_2x^2 + a_3x^3 + a_4x^4) - 1 \tag{10}$$

to obtain (the logarithm of) the correction factor for the weak line's $\tau_a(v)$.

Table 2 lists the coefficients a_0 through a_4 for 6 different values for the ratios of $f\lambda$ for the two lines (the third row corresponds to the doublet ratios that were considered in the previous examples). The coefficients other than a_1 correct for the small departures from linearity. Note that for a good general fit, $a_0 \neq 0$ even though the intercept at $x = 0$ (corresponding to no saturation at all) should be 0. The next to the last column in the table shows the largest deviations for $\log C_R$ between the results of Eq. 10 and the exact solutions to Eqs. 5 and 6 down to a minimum value of R shown in the final column. All of the coefficients vary with $f\lambda$ ratios in a smooth manner. Thus, one can obtain coefficients for arbitrary ratios between those listed in the table by interpolation.

7. Summary: Some Cautions and a Recipe

The basic principles developed in §2 and the demonstrations in §3 and §5 show that it is possible, even under fairly harsh circumstances of unresolved saturation, to derive good measurements of the column densities of absorbing substances as a function of velocity if two or more lines with different transition probabilities are observed. The analysis method proposed in this paper has a special virtue, in that it avoids the requirement for model building: one is not forced to try to reconstruct exactly what profiles should have looked like before they were smoothed by the instrument.

Obviously, how well the method works depends on a number of experimental conditions, such as ratio of $f\lambda$ of two lines, the signal-to-noise ratio of the spectrum, how well various

kinds of systematic error are controlled, and the accuracy in the match of the two velocity scales. It is not easy to give guidelines here on these issues, since there are so many possibilities. A formal evaluation of how the errors can propagate through the mathematical transformations can give some guidance. This sort of error analysis combined with common sense are probably the best tools for judging the reliability of the final results.

One must be wary of the trap where a disproportionately large fraction of the gas is located in very narrow features that are fully saturated in both lines, but where most of the absorption is caused by high-velocity fluff that is unsaturated. This condition is especially likely to arise when there is a bimodal distribution in the widths and strengths of the components in the ensemble. One should be alert for physical circumstances that could produce this state, such as lines of sight that have the right mixture of contributions from cold H I and much hotter H II regions, cases where both quiescent and shock-accelerated gases are present, or, when one is looking through entire galaxies, there is a mixture of disk and halo gases. That being said, it is reassuring to see from the demonstration in §3 that the analysis is remarkably tolerant to the existence of components that span a wide range of properties (as long as they are not too bizarre). Even a power law for the distribution of τ_0 is acceptable: see Jenkins (1986) for details.

To summarize how the correction method works, we review in the form of a recipe how one would apply it in practice:

1. For a given absorber, obtain spectra of two lines that have values of $f\lambda$ that differ by a large enough factor to show when saturation might be taking place.
2. On the basis of what the lines look like, coupled with any independent evidence (e.g. higher quality observations of other species) or a general knowledge of the physical situation, decide that the pitfall discussed in the above paragraph does not apply. If it could, do not proceed further. Also, the analysis should not be undertaken if $\tau_a(v)$ is very large (the threshold for rejection should depend on how accurately the intensities are measured).
3. For each line, measure $I_0/I_a(v)$ and evaluate its natural logarithm to obtain $\tau_a(v)$.
4. At every velocity v , use Eq. 9 to evaluate the quantity $x(v)$ from measurements of $R(v)$, the ratio of the strong line's $\tau_a(v)$ to that of the weak line, along with the two lines' $f\lambda$'s.
5. From $(f\lambda)_{\text{strong}}/(f\lambda)_{\text{weak}}$, determine appropriate values for the coefficients a_0 through a_4 from Table 2. If necessary, intermediate values can be found by interpolation.

6. For every v , evaluate the correction $C_R(v)$ by the use of Eq. 10 and the coefficients derived in the preceding step.
7. Derive the column density of the absorber per unit velocity by taking the product of the weak line's $\tau_a(v)$ and its enhancement factor $C_R(v)$, and multiplying it by the constants in front of the integral in Eq. 7. Numerically, the latter equals $3.767 \times 10^{14}/f\lambda$, if λ is expressed in Å and the column density per unit velocity has the units $\text{cm}^{-2}(\text{km s}^{-1})^{-1}$.

This research was supported by NASA grant NAG5-616 and grants GO-2403.02-87A and GO-2344.01-87A from the Space Telescope Science Institute. The inspiration for the development of the correction method described here came from data recorded by the Interstellar Medium Absorption Profile Spectrograph (IMAPS), an ultraviolet spectrograph that flew on the *Astrospace* orbital mission in September 1993. In spite of the high wavelength resolving power of this instrument, it was clear that some profiles needed to have an adjustment of their τ_a 's because they led to discrepancies in the inferred column densities for lines of different strength. The author is indebted to C. Joseph, B. Savage, K. Sembach and L. Spitzer for their useful comments on an early draft of this paper.

REFERENCES

- Barlow, M. J., Crawford, I. A., Diego, F., Dryburgh, M., Fish, A. C., Howarth, I. D., Spyromilio, J., & Walker, D. D. 1995, *MNRAS*, 272, 333
- Beals, C. S. 1936, *MNRAS*, 36, 661
- Blades, J. C., Wynne-Jones, I., & Wayte, R. C. 1980, *MNRAS*, 193, 849
- Cardelli, J. A., & Savage, B. D. 1995, *ApJ*, 452, 275
- Cardelli, J. A., Savage, B. D., Bruhweiler, F. C., Smith, A. M., Ebbets, D. C., Sembach, K. R., & Sofia, U. J. 1991, *ApJ*, 377, L57
- Crane, P., Lambert, D. L., & Sheffer, Y. 1995, *ApJS*, 99, 107
- Crawford, I. A., Barlow, M. J., Diego, F., & Spyromilio, J. 1994, *MNRAS*, 266, 903
- Ferlet, R., Laurent, C., Vidal-Madjar, A., & York, D. G. 1980, *ApJ*, 235, 478
- Fitzpatrick, E. L., & Spitzer, L. 1994, *ApJ*, 427, 232
- Hobbs, L. M. 1971, *ApJ*, 170, L85
- 1972, *ApJ*, 175, L39

- 1973, ApJ, 181, 79
- 1974a, ApJ, 191, 381
- 1974b, ApJ, 188, L67
- Hobbs, L. M., & Welty, D. E. 1991, ApJ, 368, 426
- Jenkins, E. B. 1986, ApJ, 304, 739
- Jenkins, E. B., Lees, J. F., van Dishoeck, E. F., & Wilcots, E. M. 1989, ApJ, 343, 785
- Joseph, C. L., & Jenkins, E. B. 1991, ApJ, 368, 201
- Savage, B. D., Cardelli, J. A., & Sofia, U. J. 1992, ApJ, 401, 706
- Savage, B. D., Massa, D., & Sembach, K. 1990, ApJ, 355, 114
- Savage, B. D., & Sembach, K. R. 1991, ApJ, 379, 245
- Savage, B. D., Sembach, K. R., & Cardelli, J. A. 1994, ApJ, 420, 183
- Savage, B. D., Jenkins, E. B., Joseph, C. L., & de Boer, K. S. 1989, ApJ, 345, 393
- Savage, B. D., Cardelli, J. A., Bruhweiler, F. C., Smith, A. M., Ebbets, D. C., & Sembach, K. R. 1991, ApJ, 377, L53
- Sembach, K. R., Savage, B. D., & Massa, D. 1991, ApJ, 372, 81
- Sofia, U. J., Savage, B. D., & Cardelli, J. A. 1993, ApJ, 413, 251
- Spitzer, L., & Fitzpatrick, E. L. 1993, ApJ, 409, 299
- 1995, ApJ, 445, 196
- Strömgren, B. 1948, ApJ, 108, 242
- Tripp, T. M., Sembach, K. R., & Savage, B. D. 1993, ApJ, 415, 652
- Unsöld, A., Struve, O., & Elvey, C. T. 1930, Z. Ap., 1, 314
- Vallerga, J. V., Vedder, P. W., Craig, N., & Welsh, B. Y. 1993, ApJ, 411, 729
- Vidal-Madjar, A., Laurent, C., Bonnet, R. M., & York, D. G. 1977, ApJ, 211, 91
- Wayte, R. C., Wynne-Jones, I., & Blades, J. C. 1978, MNRAS, 182, 5P
- Welsh, B. Y., Vedder, P. W., & Vallerga, J. V. 1990, ApJ, 358, 473
- Welsh, B. Y., Vedder, P. W., Vallerga, J. V., & Craig, N. 1991, ApJ, 381, 462
- Welty, D. E., Hobbs, L. M., & Kulkarni, V. P. 1994, ApJ, 436, 152
- Welty, D. E., Hobbs, L. M., & York, D. G. 1991, ApJS, 75, 425
- Wilson, O. C., & Merrill, P. W. 1937, ApJ, 86, 44

Table 2. Coefficients for Eq. 10

Ratio of $f\lambda$	a_0	a_1	a_2	a_3	a_4	Max. Residual ^a	Min. R
$2^{0.50}$	0.00096	0.29122	-0.01695	-0.03787	0.02525	-0.00096	1.07
$2^{0.75}$	0.00106	0.24182	0.01361	-0.04585	0.02407	-0.00106	1.10
$2^{1.00}$	0.00092	0.20322	0.02549	-0.04102	0.02002	0.00124	1.14
$2^{1.50}$	0.00049	0.14628	0.02569	-0.02118	0.01103	-0.00049	1.25
$2^{2.00}$	0.00022	0.10528	0.02029	-0.00755	0.00567	0.00110	1.40
$2^{2.50}$	0.00003	0.07625	0.01296	0.00128	0.00252	-0.00013	1.70
$2^{3.00}$	0.00001	0.05413	0.01043	0.00249	0.00183	0.00022	1.90

^aDefined as $\log(C_R)_{\text{exact}} - \log(C_R)_{\text{Eq. 10}}$ over the range $\text{Min}(R) < R < \text{Ratio of } f\lambda$.